Composite Sorbent Prepared from Layered Double Hydroxide Nanoparticles to Remediate Simulated Groundwater Polluted with Lead and Cadmium Ions

Teba S. Hussein[*] , Ayad A.H. Faisal

Department of Environmental Engineering, University of Baghdad, Baghdad 10001, Iraq

Corresponding Author Email: teba.hussein2011d@coeng.uobaghdad.edu.iq

ABSTRACT

This study presents a novel composite sorbent, synthesized from industrially inexpensive and abundant materials, designed for the remediation of groundwater contaminated by lead (Pb) and cadmium (Cd) ions through a permeable reactive barrier (PRB) technique. The synthesis process innovatively employs alum, a low-cost compound, alongside plaster kiln dust — a by-product waste from the gypsum industry — and Cetyl trim ethyl ammonium bromide (CTAB), to produce Nano-sized layered double hydroxide (LDH) composed of aluminum (Al^{+3}) and calcium (Ca^{+2}) ions. The synthesized LDH gel-solution was characterized using X-ray diffraction (XRD) analysis and subsequently intercalated onto an iron-slag surface, yielding a novel sorbent termed "iron-slag coated with (Ca/Al-CTAB)-LDH". The intercalation of CTAB and the presence of LDH nanoparticles significantly increased the iron-slag surface area from 0.48802 to 10.21 m^2/g, thereby enhancing the adsorption capacity of the sorbent for Pb and Cd ions. Optimal synthesis parameters were identified as 0.035 g/50 mL CTAB, pH 10, (Ca/Al) molar ratio of 2, and an iron-slag dosage of 1 g/50 mL. Long-term column tests, spanning a duration of at least 25 days, were conducted, revealing a marked increase in the sorbent's longevity in the packed column when a low flow rate and inlet concentration of contaminants were combined with a high mass of sorbent. The experimental data from the breakthrough curves were successfully fitted by several models, including Bohart-Adams, Thomas-BDST, Yan, Belter-Cussler-Hu, and Clark expressions, with a determination coefficient (R^2) exceeding 0.99 and a sum of squared errors (SSE) less than 0.162. The hydraulic conductivity of the packed sorbent remained largely constant at 2.7×10^{-2} cm/s, suggesting its suitability for PRB applications. The prepared sorbent demonstrated high efficacy in the removal of Pb and Cd ions from contaminated water, making it a promising tool for environmental remediation.

1. INTRODUCTION

Life on earth is sustained by soil, an invaluable and non-renewable resource [1]. However, anthropogenic activities have precipitated extensive soil degradation and pollution [2]. Heavy metals, a group of toxic metals and metalloids, pose significant threats to ecosystems and human health due to their presence in soil [3, 4]. Issues surrounding heavy metal contamination in groundwater and soil, propelled by rapid industrialization and urbanization, have garnered significant attention in recent times. These metals can bioaccumulate in plants and animals, subsequently infiltrating the human food chain.

Despite the diverse chemical properties of heavy metals, their non-biodegradable nature and inorganic composition render them as persistent environmental hazards when released into ecosystems. Metals such as cadmium, mercury, lead, chromium, cobalt, copper, nickel, and zinc are particularly detrimental to environmental health [5]. They are often introduced into the environment through mismanaged industrial waste and mine tailings, posing a global environmental risk. Mine tailings, in particular, often contain high levels of heavy metals, resulting in soil and groundwater contamination [6].

Recent global studies have underscored the severity of heavy metal pollution in groundwater, emphasizing the necessity for ongoing development of treatment technologies. Consequently, the primary objective of this study is to design and synthesize novel reactive materials that meet key requirements for permeable reactive barriers (PRBs), particularly with regard to groundwater flow and contaminant sequestration [7].

Layered double hydroxides (LDHs) have drawn significant interest in their synthesis phase due to their potential applications in diverse fields such as electrochemistry, magnetism, and environmental science. LDHs are cost-effective and simple to produce on both laboratory and commercial scales, making them an attractive reactive medium for various anions [8], cations [9], radionuclides [10] and dyes [11].

The gypsum industry produces large amounts of plaster kiln dust by-product waste, and the steel and iron industries generate significant quantities of iron-slag, a byproduct that amounts to approximately 50×10^6 tons annually. These industrial wastes can be repurposed to produce new sorbents for treating contaminated water, exemplifying the sustainable

and green synthesis approach that mitigates the adverse impacts of industrial by-products and processes on the environment and human health. Alum, or aluminum sulphate, is a low-cost coagulant commonly used in water treatment processes and can also contribute to the creation of the proposed coated slag.

Therefore, this study aims to produce LDH nanoparticles through a chemical reaction involving calcium (extracted from the readily available and inexpensive by-product, plaster kiln dust) and aluminum (derived from alum dissolution), in the presence of a well-known surfactant (cetyltrimethylammonium bromide, CTAB). These particles are then precipitated onto the surface of iron-slag to create a "coated slag". The performance of this coated slag is subsequently evaluated for its potential use in PRBs to limit the propagation of contamination plumes.

2. EXPERIMENTAL APPROACH

2.1 Materials

Plaster Factory located in Iraq was the source of PKD utilized in this work, the principal core of this study is to extract the calcium from PKD waste instead of its disposal to the ambient environment. The PKD is heterogeneous matter because it includes particles of various sizes; therefore, sieving is necessary to select particle sizes between 0.6 and 1 mm [12], with existence of CTAB surfactant to produce "iron-slag coated with (Ca/Al-CTAB)-LDH". CTAB is the organic cationic surfactant that was supplied in powder by Sigma Aldrich Chemise (Germany). The intercalation of this surfactant has a high role in the enlargement of the LDH interlayers and, consequently, significant increase in the surface area can be occurred. calcium must be mixed with aluminum resulted from addition of alum (aluminum sulphate) at the room temperature.

Iron and steel factory in Babylon Governorate-Iraq, produced iron slag byproduct. To get rid of the fine powder, slag must be cleaned with distilled water (DW) and; then, dried for 24 hours at 105 degrees Celsius. The properties of this byproduct have been measured at the Material Research Laboratories - Ministry of Science and Technology; Petroleum Development and Research Centre- Ministry of Oil; and Iraqi Geological Survey. The particles utilized in this study have sizes ranging from 0.6 to 1 mm; therefore, a geometric size of 0.775 mm. For iron, bulk density, hydraulic conductivity, porosity, pH, ash content, and BET surface area have values of 2.026 g/cm^3, 2.69 x 10^{-3} m/s, 0.41, 8, 10% and 0.2571 m^2/g respectively. In this investigation, lead (Pb^{+2}) and cadmium (Cd^{+2}) were the target contaminants. By dissolving 1.5985 grams of lead nitrate in 1 L DW, a stock solution with Pb^{+2} content of 1000 mg/L was created. Also, stock solution (1000 mg/L) of Cd^{+2} was prepared by dissolving certain of cadmium salt in DW. The two solutions must be preserved at temperature of room, and pH can be changed by addition 1 M NaOH or HCl as needed to prevent lead and cadmium ions from precipitating.

2.2 Fabrication of sorbent

CTAB surfactant is mixed with calcium and aluminum, in order to produce nanoparticles of LDH that are planted on the surfaces of the slag by co-precipitation and given the name "coated slag". This composite sorbent's capacity in the Pb^{+2} and Cd^{+2} ions capturing from wastewater can serve as a useful guide for determining the optimal CTAB, Ca/Al ratio, solution pH, and iron slag dosage for its production. The following provide an explanation of the present composite sorbent's preparation.

One hundred milliliter of distilled water contained 1.5 mL of ten percent (v/v) HCl was mixed with one gram of PKD. Resulted solution must agitate at 250 rpm for three hours in room temperature, and filtration by filter papers can isolate solid (filter) cake from aqueous solution rich with Ca^{+2} ions. Specific weight of alum must be dissolved in DW, then the calcium solution must be mixed with the aluminum solution to prepare the final solution that have different molar ratios of Ca/Al like 1, 2, and 3. Different dosages of Cetyl trimethyl ammonium bromide (CTAB) were added (0.03, 0.035, 0.05) g to 50 mL of solution to increase surface distance between interlayers. Iron slag is added to 50 mL of solution in different doses (0.5, 1, and 1.5 gram). Drops of sodium hydroxide (1 M) were employed for raise the pH to various values of pH (9,10, and11) to produce a coated layered of (Ca/Al- CTAB)-LDH on surfaces of iron slag, and flasks were stirred at 250 rpm for 3 hours. Solution was sonicated for 10 min in ultra-sound to smoothing and disperse nanoparticles. Coated iron slag should be separated from the centrifuged solution, and this iron slag could be air dried at 60°C for 24 hours to generate the needed composite sorbent for eliminating cadmium and lead contaminants. The maximum value of adsorption capacity has employed as an indicator to determine the efficacy of the coating process under influences of solution pH, (Ca/Al-CTAB) molar ratio 2, pH 10, CTAB 0.035 g, and iron slag 1g dose.

2.3 Characterization analyses

The "Siemens X-ray diffractometer, D8 Advance, Brucker, Germany" was used for the XRD analysis to examine the manufactured sorbent's crystalline structure. Functional groups liable for pollutant restricting with composite sorbent can be determined through FT-IR investigation. Additionally, the "X Flash 5010, Bruker AXS Microanalysis, Berlin, Germany" SEM-EDS test is used to determine the sorbent's morphology and element percentages.

3. COLUMN TESTS

Laboratory column experiments were completed to evaluate the permeability and reactivity of the covered slag in order to verify the geochemical and hydraulic performance of the produced sorbent. Figure 1 shows experimental simulation experiments using the column technique that reflect a one-dimensional model of the barrier's real operation and column setup. Two aspects—contaminant elimination effectiveness, coated slag durability, and hydraulic conductivity—were examined in order to assess the reactive medium's efficacy in PRB. The adsorbent continuous setup that was used in this work was made of two PVC columns that were arranged in a row-like fashion, along with a number of accessories like a water holding tank, a peristaltic pump, valves, and pipelines. Each column's wall is 5 mm thick, with a 50-centimeter height and a 2.5 cm interior diameter. To test the efficacy of (Ca/Al-CTAB)-LDH nanoparticles in reducing contaminants content, an iron-slag-coated column was filled.

Distilled water was poured into the slag layer at room temperature from the bottom up to prevent the incidence of trapped air. A particular hydraulic gradient was used to introduce contaminated water to the bed at a rate of 5, 10, or 15 mL/min once saturation was reached. Each column has openings 1, 2, and 3 that are situated 10, 30, and 40 centimeters, respectively, from the inlet. Outlets have been used to remove samples of purified water at predetermined intervals to check the level of metals.
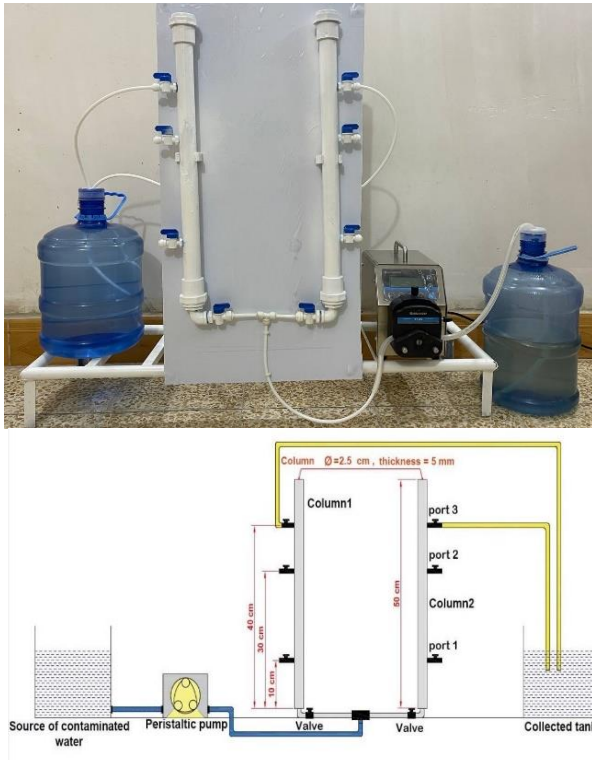
Figure 1. Components and configuration of column set-up used for continuous operation; schematic diagram of column set-up used for continuous operation

4. MODELING OF BREAKTHROUGH CURVES

The behavior of a fixed-bed column is described by the propagation of the breakthrough curves. The tendency of the breakthrough curve and the duration of the breakthrough process have a significant impact on the operation and dynamic reaction of an adsorption column [13]. A collection of algebraic models can mimic curves:

4.1 Thomas model

It is one of most general and widely used models in previous studies such as the study [14]. In order to derive this model, it was assumed that the Langmuir model would explain the sorption approach without taking into account dispersion in the axial direction and that driving force would be a second-order kinetic reversible reaction. Thomas model can be written as follows [15]:

$$\frac{C}{C_0} = \frac{1}{1 + \exp\left[\frac{(Mq_0K_{Th})}{Q} - \frac{K_{Th}C_0t}{1000}\right]} \tag{1}$$

where, M is sorbent mass filled in column (in grams), Q is flow rate of water pumped into the bed (in milliliters per minute), C_o is influent or inlet concentration (in mg/L), q_o is maximum sorption capacity (in mg/g) and K_{Th} is Thomas rate constant (mL/min mg). This model can be used to estimate values of q_o and K_{Th} by fitting measured breakthrough curve with non-linear regression of Excel 2016.

4.2 Belter model

This model proposed by the study [16] is semi-empirical formula used to describe the breakthrough curves for fixed bed in the packed column:

$$\frac{C}{C_o} = 1 + \text{erf}\left[\frac{(t - t_o)\exp\left(-\sigma\left(\frac{t}{t_o}\right)\right)}{\sqrt{2}\sigma t_o}\right] \tag{2}$$

where, t_o is the time identical to C/C_o equal to 50% (min) and σ is the standard deviation which represents the slope of breakthrough curve.

4.3 Yan model

This model was also known as the "Dose-Response model" in earlier research, and its expression can be found in Eq. (3) [14, 17]:

$$\frac{C}{C_0} = 1 - \frac{1}{1 + \left(\left(\frac{Q \times C_0}{q_0.M}\right) \times t\right)^a} \tag{3}$$

where, Q is influent contaminated water's flow rate in L/min and a is the slope of curve between C/C_o and t. In Microsoft Excel 2016, non-linear fitting can be used to estimate the constants q_o and a.

4.4 Bohart-Adams model

It forms the one of the first mathematical expressions used to relate between C/C_o and time for 1-D bed. The main assumptions used in derivation of this model are [14, 17]. i) the model can describe the lowest concentrations, ii) the saturation concentration can be achieved as time goes to infinity, and iii) the external mass transfer can specify the speed of adsorption. This model can write as follows [17]:

$$\frac{C}{C_o} = \frac{1}{1 + \exp\left(KN_o\frac{Z}{U} - KC_ot\right)} \tag{4}$$

where, Z is bed depth (cm), t is elapsed time (min), U is rate of flow (cm/min), K is kinetic constant (L/g/min), N_o is the content of solute at saturation level (mg/L),

4.5 Clark model

Sorption trend of chemical species in this model follows Freundlich isotherm and flow is of piston type; however, following kinetic equation was developed [18, 19]:

$$\left(\frac{C}{C_o}\right)^{n-1} = \frac{1}{1 + A \cdot e^{-rt}} \tag{5}$$

where, *r* and *A* are constants of the kinetic formula while *n* is the exponent of Freundlich model.

5. RESULTS AND DISCUSSION

5.1 Manufacturing of sorbent

Four specific parameters have an impact on the manufacturing of "iron-slag coated with (Ca/Al-CTAB)-LDH". On the prepared sorbent, the CTAB mass, aqueous solution pH, molar ratio of Ca to Al, and iron-slag mass have all been investigated. The appropriate indicators that can be utilized to determine the best magnitudes of the aforementioned parameters were those with the highest adoption contaminant removal efficiencies. In order to produce coated slag, three CTAB masses 0.0, 0.035, and 0.05 g were used in conjunction with a pH of 10 and ration of Ca/Al 2 and a mass 1 g of iron slag per 50 milliliters. For the purpose of determining how this coated slag would react with an aqueous solution that was tainted with Pb^{+2} and Cd^{+2} ions, sorption tests have applied with Co 50 mg/L, pH 5, sorbent mass 0.5 g/50 mL, time period of three hours, and speed of agitation 250 rpm.

The existence of CTAB, which has significant effect in increasing the spacing for Ca/Al inter-layer and can improve the adsorptive characteristics of prepared slag, may be the cause of this increase in removal efficiency. Forces of electrostatic repulsion can generate between the cations present in the synthesized slag and the contaminant can result in a significant decrease in the amount of metal removed [20].

Preparation tests were carried out with three pH values — specifically 9, 10, and 11 - at the same values of synthesis and sorption conditions mentioned in the study to determine the effect of CTAB mass, with the exception of the mass of surfactant, which must be taken the best one (=0.035 g). According to the measurements, the solution pH of 10 has the highest removal efficiency. Due to the fact that not all nanoparticles will adhere to the iron-slag or because the diameter of the nanoparticles is increasing, the removal percentage can be slightly reduced by increasing or decreasing the pH from 10; consequently, the coating process at pH 10 is optimal [21].

For same conditions of sorption tests, three values of this ratio specifically 1, 2, and 3 were used. An increase or decrease in this molar ration can be resulted in a decrease in Pb^{+2} and Cd^{+2} ions removals. LDH's disordered, hydrotalcite-like composition or variations in the radius difference between Al and Ca could be the primary cause of this decrease in removal efficiency [22].

The final parameter examined in the synthesis of the current sorbent was the iron slag dosage. Three different slag masses 0.5, 1, and 1.5 g/50 mL on the production of composite sorbent under the same optimal preparation conditions. It seems that the 1 g of slag per 50 mL of solution utilized to prepare coated slag can remove the maximum quantity of Pb^{+2} and Cd^{+2}. A decrease in the quantity of iron slag can associate with a clear decrease in the metal removal; this can explain by the fact that many (Ca/Al-CTAB) nanoparticles do not have the opportunity to adhere with iron slag; as a result, they will be washed away. Additionally, the increase in surface area for the same quantity of nanoparticles as compared to the best one may be the cause of the decrease in removals for iron slag dosages greater than 1 g.

5.2 Description of present sorbent

The "X-ray diffraction (XRD) analysis" is very essential for specifying and identifying the mineralogical composition of materials used in the preparation of present sorbent. In Figure 2(a), the PKD, virgin iron-slag, and coated iron-slag XRD patterns were displayed. In order to create a plot relating the intensity of the diffracted beam to two Theta (2θ), the material sample in this test is subjected to a collimated beam of parallel X-rays and diffracted beams of varying intensities. With Cu K radiation and an X-ray diffractometer (40 mA, 40 kV), the records with 2θ ranged from 5° to 80°. Based on International Centre for Diffraction Data, ICDD databases, the XRD pattern of PKD had peaks that correspond to many compounds like gypsum, montmorillonite, calcium sulfate, iron oxide, and quartz as shown in Figure 2(a). Also, this figure certifies the presence of many metal oxides in the composition of iron slag like manganese (MnO), aluminum (Al_2O_3), calcium (CaO), iron (Fe_2O_3), and silica (SiO_2). Depended on the "Joint Committee on Powder Diffraction Standards, JCPDSs", the XRD analysis for coated slag proved the appearance of several reflections at intensities of 22.693, 25.501, 31.741, 34.081, 38.865, 40.983, 45.469, 48.589, 52.541, 56.467, 57.317, and 78.983 which identical to the nanoparticles of Ca+ Al + CTAB precipitated on the slag surfaces. The formation of new sites on the coated sand can be supported the removal of Pb^{+2} and Cd^{+2} ions onto the prepared sorbent [23].
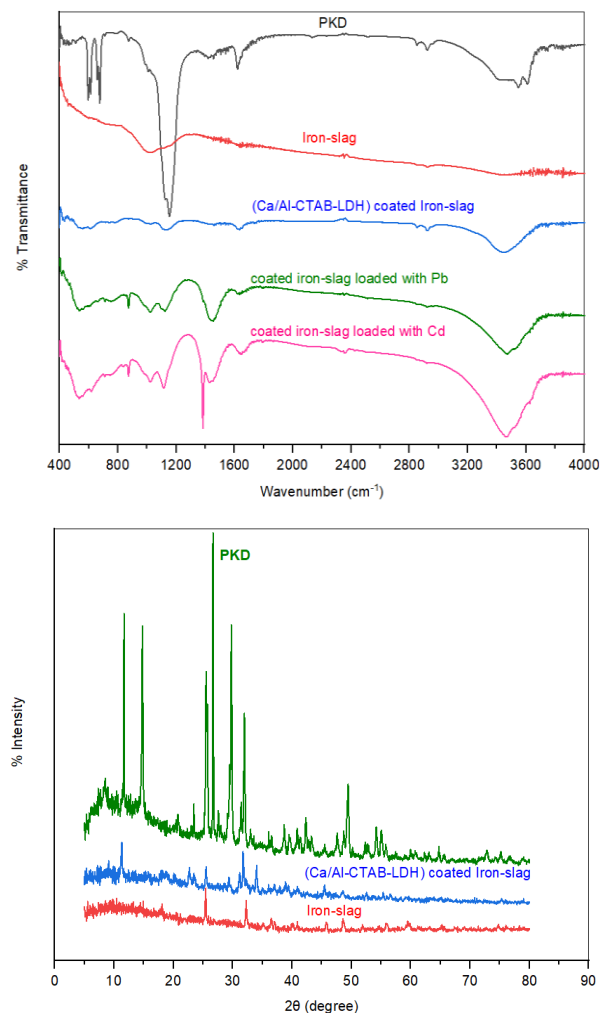
Figure 2. X-ray diffraction (XRD) analysis; FT-IR analysis

The results of the FT-IR analysis for wavenumbers ranging from 400 to 4000 cm^{-1} (Figure 2(b)) was used to identify the working functional groups for PKD, coated iron slag, coated iron slag loaded with Pb^{+2} and Cd^{+2} ions, and virgin iron slag. According to the spectra, the OH group is represented by a broad and strong peak at wavenumber 3442.3 cm^{-1} [24]. The C–C group vibration can be linked to peak values of 554.4, 675.93, 704.9, 811.8, and 894.7 cm^{-1} that were found. C–O group vibration can be used to identify the peak values of 1149.4, 1260.25, 1265.07, 1290.14, and 1308.5 cm^{-1} that were identified [25]. At 1560.13 cm-1, an olefinic C=C stretching band can be seen, and its conjugation with a C=O or C=C bond can cause a clear shift to lower wavenumbers. As a result, the principal functional groups found in the current materials are O–H, C=C, C=O, C-C, and C–O. Appearance of peaks at 2345.16 and 2358.5 cm^{-1} demonstrated to the existing of C-N vibration in tertiary amines. The removal of Pb^{+2} ions onto coated iron-slag is mainly controlled by electrostatic interaction and hydrogen bonding, according to the FT-IR spectrum of a reactive material's chemistry.

As shown in Figure 3, FESEM graphs are useful for describing the morphological characteristics of PKD, virgin iron slag, coated iron slag, and coated slag loaded with lead and cadmium ions. Iron slag's porous surface exhibits irregular morphology, giving the impression of roughness and cracks. The formation of layers with irregular orientations and sizes is depicted in Figure 3(a) [26, 27]. However, the sorbent's efficiency at capturing lead and cadmium ions can be improved by increasing the surface area exposed for interaction. In contrast to the sorbent before the interaction with metal ions (Figure 6 (b)), the sorbent's morphology changed clearly (Figure 3 (c, d)) after the binding of lead ions. The findings of the BET surface area test proved that the current sorbent had a significant increase in area, going from 0.488 m^2/g for iron-slag to 10.21 m^2/g after the coating process.
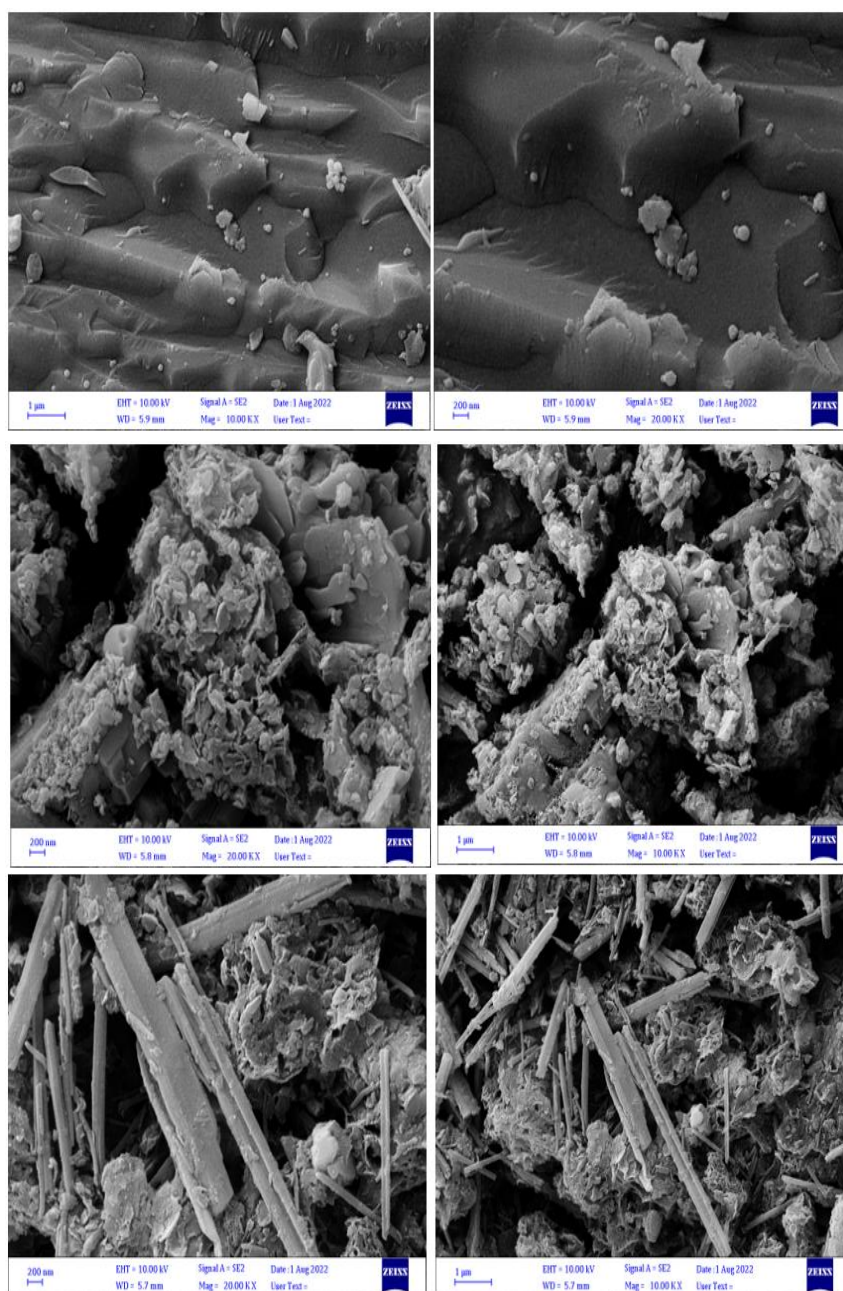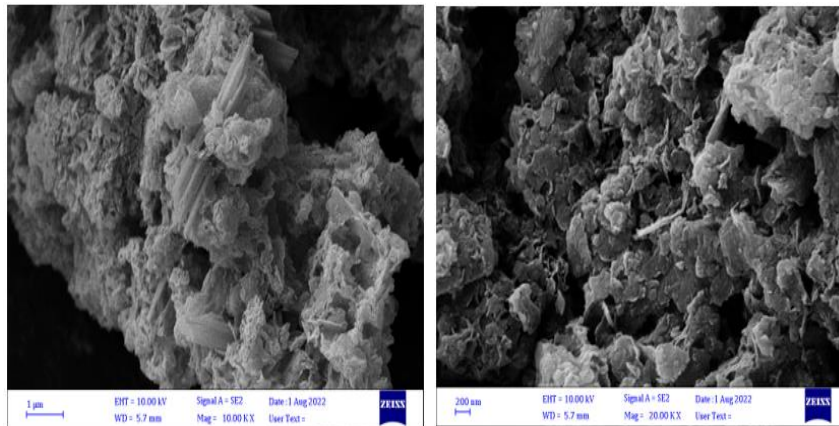
Figure 3. FESEM images for virgin iron-slag; coated iron-slag; coated iron-slag loaded with Pb^{+2} ions; and coated iron-slag loaded with Cd^{+2} ions

As depicted in Figure 4, EDS produces elemental composition graphs for PKD, virgin iron-slag, and composite sorbent before and after the sorption process. Representative iron slag grains clearly contain Ti, O, Si, Fe, k, Al, C, Ca, Mg, Na, and Mn as major elements. According to the tables in Figure 4, the coated iron slag contained 18.0 and 17.7 percent Ca and Al, respectively. This rise demonstrates the plantation's success with layered double hydroxides. As illustrated in Figure 4(c, d), interaction with iron-slag particles can result in the formation of a cloud of lead and cadmium ions.
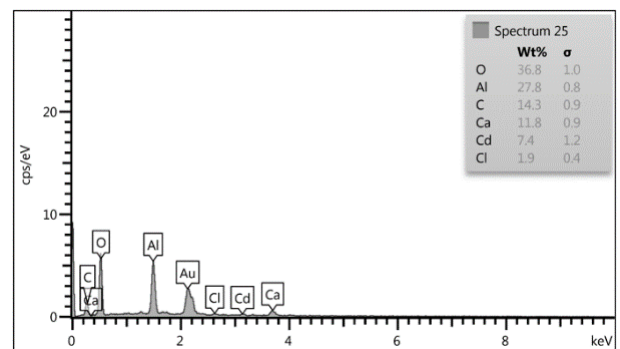
Figure 4. EDS images for virgin iron-slag; coated iron-slag; coated iron-slag loaded with Pb^{+2} ions; and coated iron-slag loaded with Cd^{+2} ions
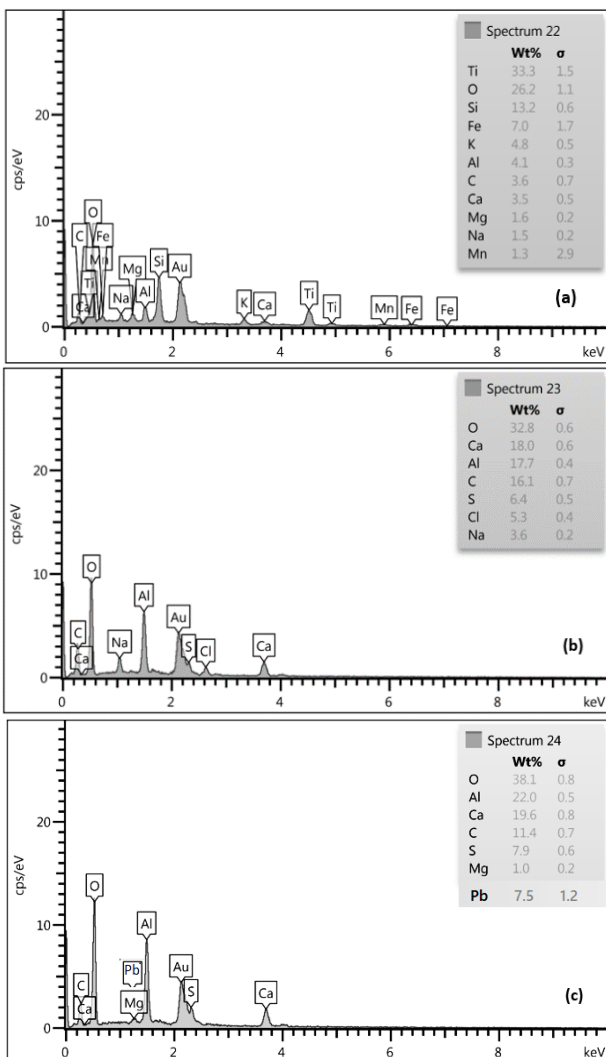
5.3 Performance of coated slag bed

Using coated slag as the PRB, the movement through the column arrangement was evaluated. The goal of the tracking is to determine how well the barrier performs in removing the heavy metals lead and cadmium from aqueous solutions while keeping a reasonable hydraulic conductivity coefficient under changing inlet concentration, water flow rate, and mass of coated slag. Figure 5 illustrates the effect of the input percentage of adopted metals through the barrier bed at a flow rate of 5 mL/min for ports 1, 2, and 3. Variations in the concentration gradient may have an impact on the bed's rate of absorption. Due to the incidence of delayed sorption, it appears that the form of the curve is less obvious at lower influent concentrations. However, as influent concentration rises and the sorbent becomes saturated, the slope steepness of the parabola increases. Additionally, low concentration gradients cause chemical species to propagate slowly through pores because the mass transfer coefficient is reduced [28], which extends the time for saturation. The breakthrough time corresponded to 5% of the normalized concentration (C/Co) for adopted contaminant can be specified from the plotted curves and this time represents the bed longevity to ensure the outlet concentration below the acceptable limit. For example, Figure 5 port 1 (a-c) for Pb^{+2} contaminant certified that the breakthrough time for bed depth of 40 cm (P3) was equal to 180 h when inlet concentration of 50 mg/L and flow rate of 5 mL/min; however, this time was decreased significantly to become 120 and 84 h for 100 and 150 mg/L respectively. The lowest longevity (≈42 h) can be occurred at P1 when inlet

concentration of 150 mg/L for mentioned flow rate, the relationship between "breakthrough time" and "inlet concentration" can be seen to follow a similar pattern. Due to difference in affinity and adsorption capacity of Pb and Cd with coated iron-slag, the longevities of the barrier in the case of Cd were smaller than that of Pb.

b) Port 2, Q=5 mL/min, Co= 100 mg/L

c) Port 2, Q=5 mL/min, Co= 150 mg/L

a) Port 3, Q=5 mL/min, Co= 50 mg/L

b) Port 3, Q=5 mL/min, Co= 100 mg/L
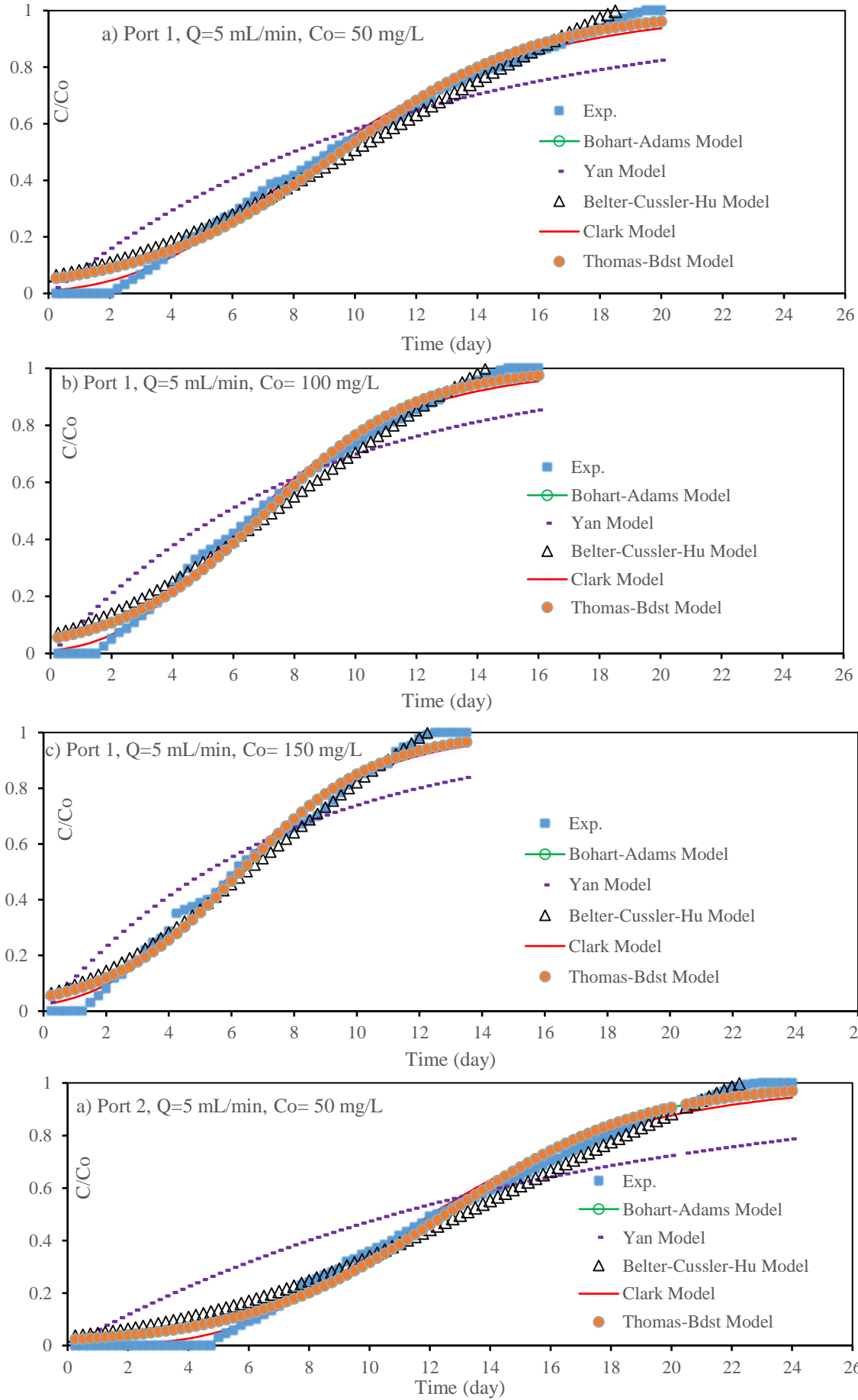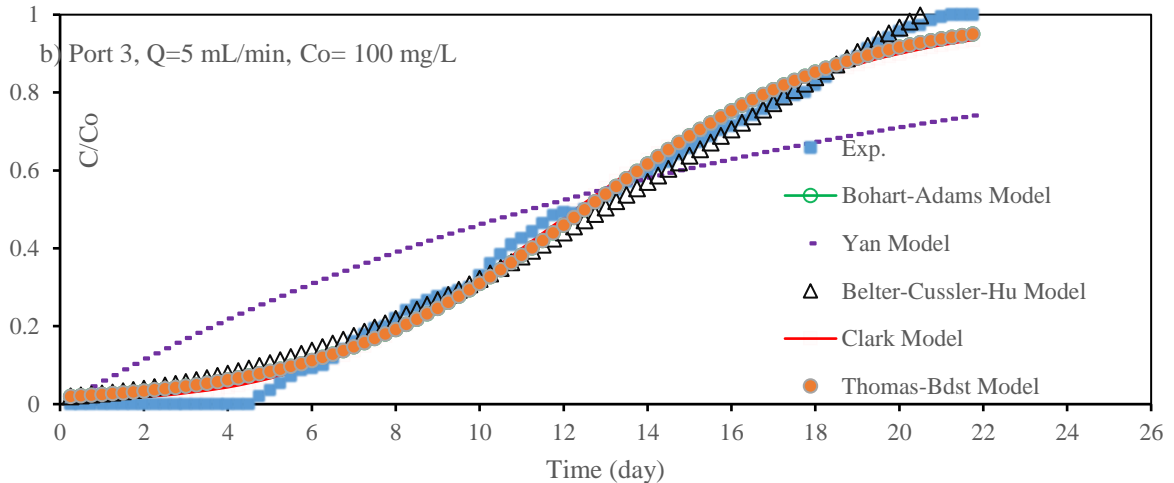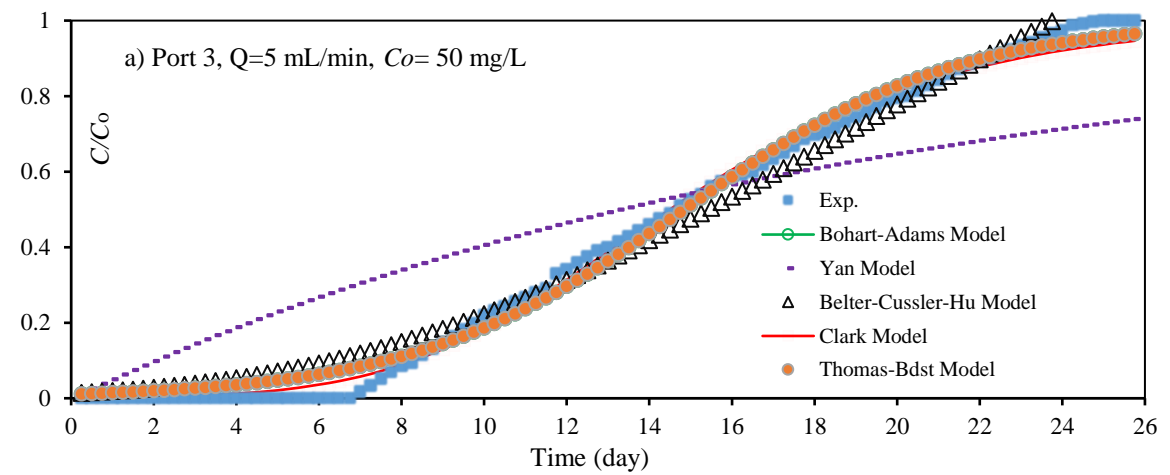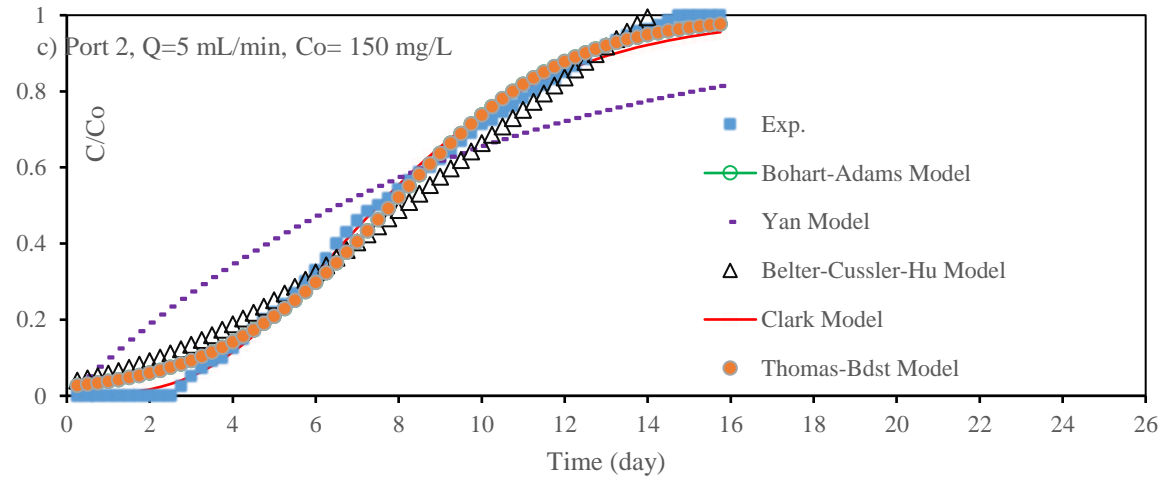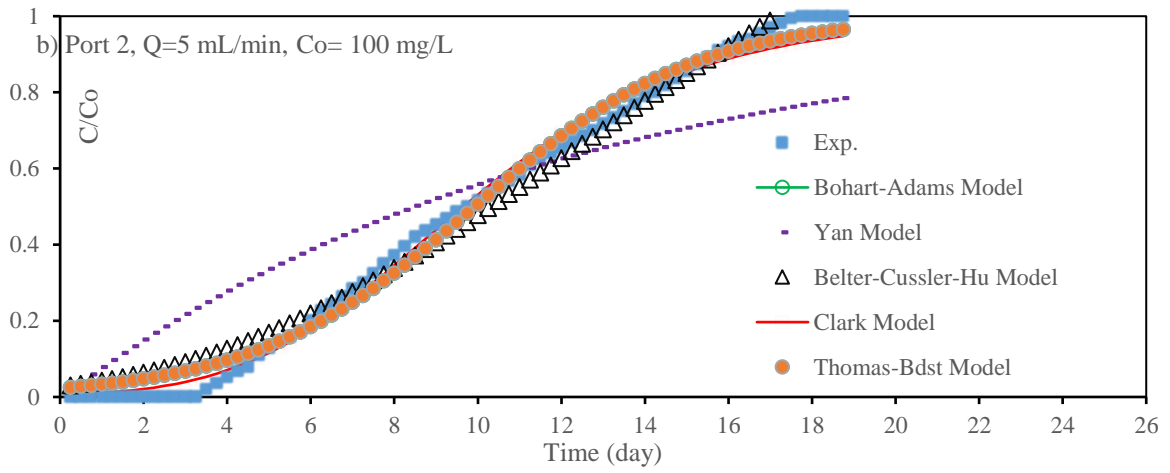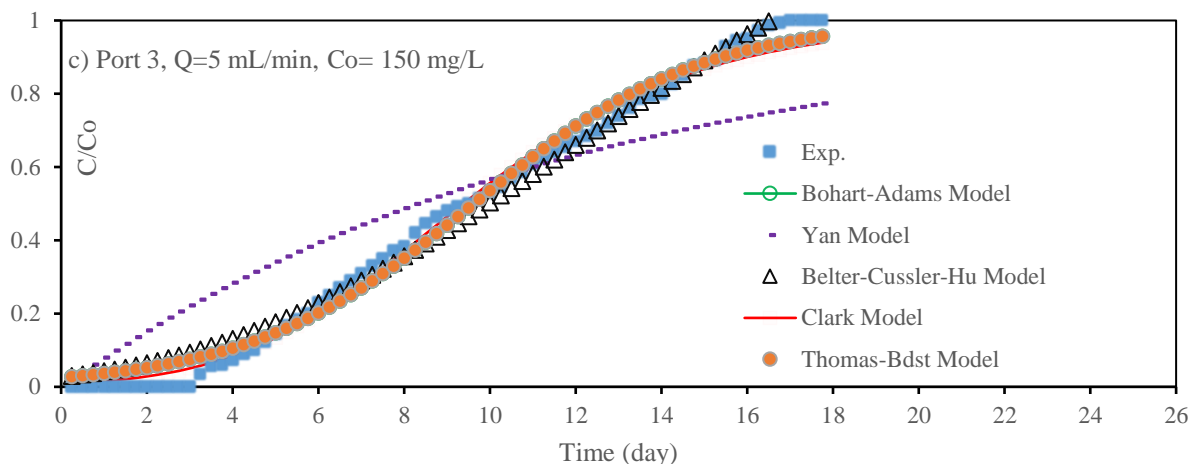
Figure 5. Measured breakthrough curves of Pb^{+2} ions in comparison with predictions of models for different inlet concentration at ports 1, 2 and 3

Applying three rate values 5, 10, and 15 mL/min to the sorption of Pb^{+2} and Cd^{+2} onto covered slag barriers allowed for monitoring the effect of water flowrate on that sorption. Plots of breakthrough curves (Figure 6) were made using the aforementioned flow rates at Ports 1, 2, and 3 and an input concentration of 50 mg/L. It is obvious that a higher discharge will result in shorter breakout times and steeper slopes. Thus, the influent metal molecules depart before reaching the equilibrium state [29] because the retention period is insufficient. As water velocity rises, solute adhesion to solid particulates decreases, which may result in a noticeable decline in clearance percentage [30]. As a consequence, the solute's retention period in the packed bed was insufficient to allow for the achievement of sorption equilibrium at a particular discharge. As a result, the solute will exit the bed before it has an opportunity to bind to the coated slag's active sites. Furthermore, reversible and porous interactions between the sorbent surface and some of the connected solute molecules may make some of the molecules desorbed under high flow rates. As a consequence, the metal content in effluent quickly rises, which causes an early breakthrough time. In the case of inlet Pb content of 50 mg/L at Port3, increasing flow rate from 5 to 15 mL/min can result in a notable reduction in breakthrough time of 180 to 72 h; however, the same reduction in time (156 to 42 h) can be noted for Cd under the same circumstances. Because the chemical will exit the bed before it achieves equilibrium, an increase in discharge will hasten the emergence of the chemical front, reduce "breakthrough time," and steepen "breakthrough curves." A chemical equilibrium is defined as the absence of an observable change in the system after a period of time.

It is clear in the graph mentioned that the adsorption rate was very fast initially and it's increased with increasing of contact time until reached the equilibrium time. indicating a gradual blinding of sorption sites on the adsorbent surface. While the residual concentrations of these chemical species are being kept relatively constant with insignificant can't changes. The high rate of adsorption can be attributed to the existence of adequate numbers of the reactive binding sites on the sorbent surface. This means that the amount of these contaminants sorbed per unit mass of sorbent decreased with the increase in initial concentration. This represents saturation of the active sites available on the iron-slag samples for interaction with contaminants, indicating that less favorable

sites became involved in the process with increasing concentration. For weak and reversible bonds, the high discharge may also desorb many attached molecules from the sorbent surface. As a result, the effluent's metal concentration rises rapidly, accelerating the "breakthrough time", low flow rate helped removal of metals in the packed bed due to its higher capacity of adsorption. Present results were in agreement with those reported in previous studies [31, 32].

Figures 5 and 6 for Pb^{+2} demonstrate that bed depth can affect the spread of contaminant fronts, with a notable delay in the emergence of the metal fronts due to an increase in the amount of sorbent material compressed in the column. This implies that a deeper layer provides solute molecules enough time to diffuse within particle holes, increasing the amount of metal that is adsorbed. These figures display standard S-shaped breakthrough curves, which indicate a rise in collected effluent and breakthrough duration with bed depth. For a flow rate of 5 mL/min and a concentration of 50 mg/L at intake, the "breakthrough time" can significantly rise from 2.25 to 7 days (Pb) and from 1.75 to 6 days (Cd) with a change in bed depth from 10 cm (Port 1) to 40 cm (Port 3). It is essential to note that, for a given inlet concentration, increasing bed depth will result in a reduction in bed adsorption capacity because, at a greater depth, a given amount of metal can spread over a larger surface area. Sorbents become depleted, that is, they reach a point where they are no longer able to remove molecular species. Time lapse taken to attain this exhaustion stage is called "exhaust time", at which effluent C/C_o equals to 0.9. This time is increased with higher bed height because of presence of more active sites for adsorption. Capacity of adsorption for higher bed height is decreased because of; i) overlap of active sites can be limited their effective use in the removal of chemicals [32], and ii) generation of channels especially in the region between the wall of column and packed bed; so, the solution will find its way to escape from the bed without treatment.

Metals ions breakthrough curves along coated slag bed at different discharges and inlet concentrations for depths ranging from 10 to 40 cm are compared with experimental measurements in Figures 4 and 5. Bohart-Adams, Thomas-BDST, Belter-Cussler-Hu, Yan and Clark models were used to simulate these curves at ports 1, 2, and 3. "solver option in Microsoft Excel 2016 for nonlinear regression" was applied to determine fit between the models mentioned and the

measurements. Also use mathematical simulation for experimental measurements of breakthrough curves using advection-dispersion-sorption equation, which is solved numerically by finite element method with the aid of Computer Solution (COMSOL) software. Very similar results were obtained with satisfactory agreement between the two methods.

The output of fitting process (like parameters of models with measures of goodness) has been listed in Tables 1 and 2 for cadmium. With the lowest sum squared errors (SSE) and higher coefficient of determination, the Bohart-Adams, Thomas-BDST, Belter-Cussler-Hu, and Clark models accurately describe the experimental measurements.

Hydraulic conductivities of coated slag packed in column at various time intervals were calculated using hydraulic gradient and accumulative volume of treated water. Results showed that hydraulic conductivity coefficients remained relatively constant throughout experiments, with a mean value of $2.7*10^{-2}$ cm/s. The fact that there is a low likelihood of precipitate formation within packed bed can be used to explain this behavior. Additionally, gaps accessible for the movement of aqueous solutions retain their accessibility in the transfer of solution and, subsequently, dissolved metals along bed. For mattresses in PRB, conductivity must be higher than $2.1*10^{-2}$ cm/s.
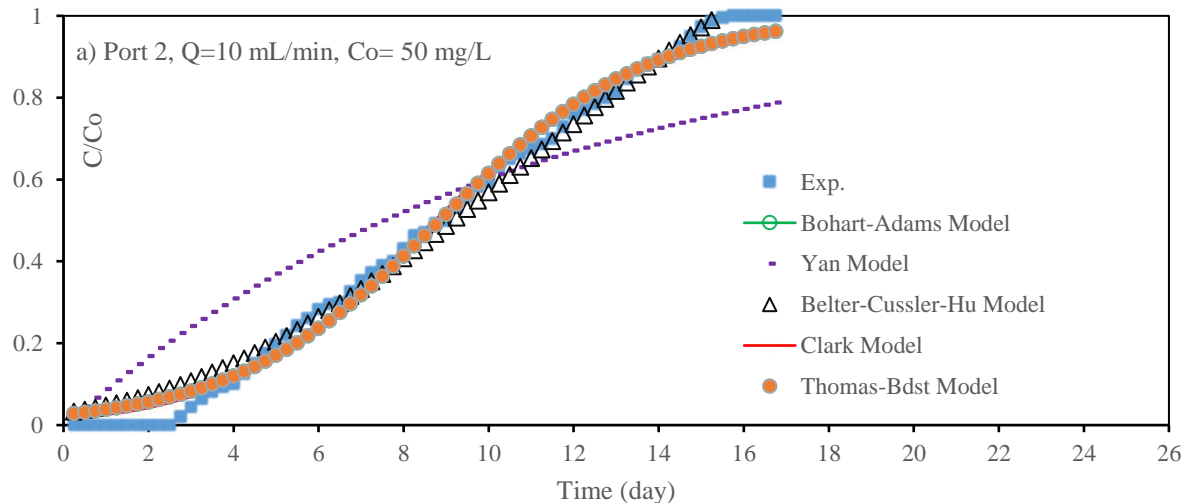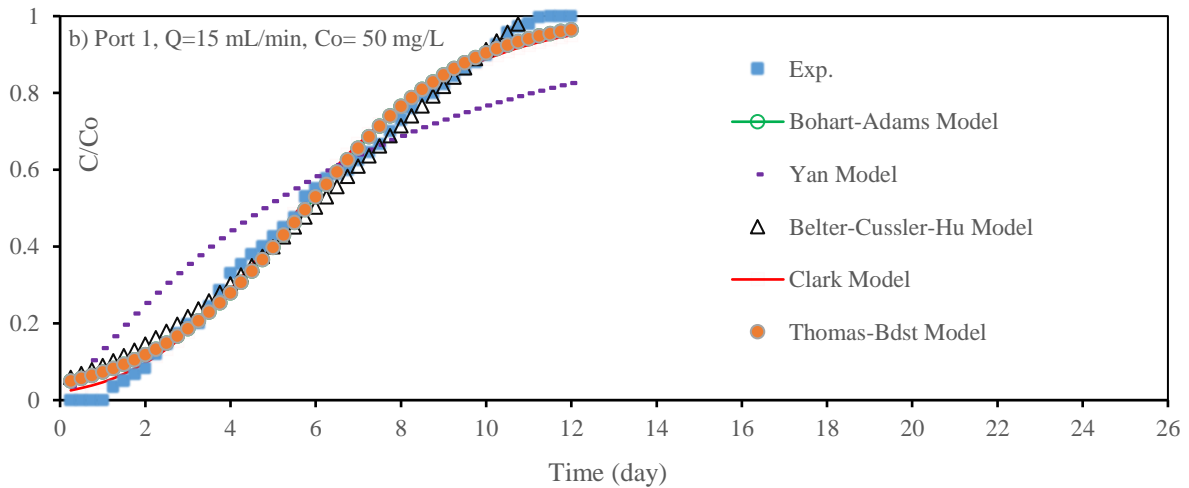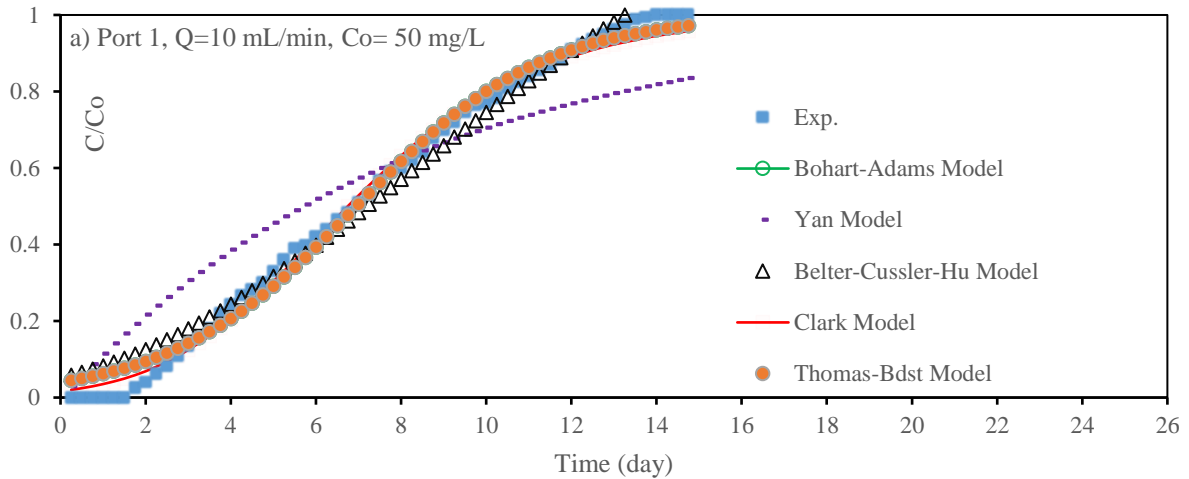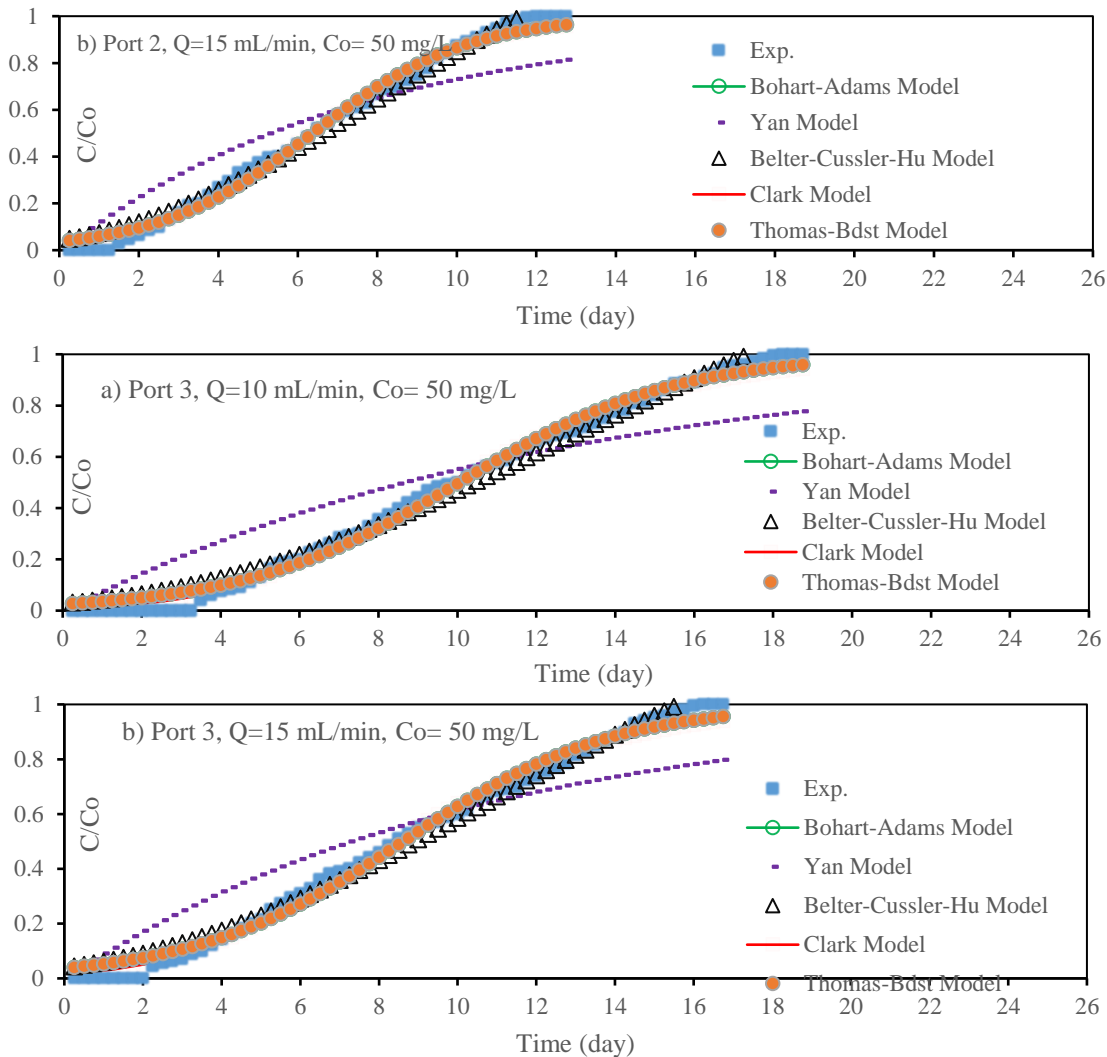
Figure 6. Measured breakthrough curves of Pb^{+2} ions in comparison with predictions of models for different water flow rates at ports 1, 2 and 3

Table 1. Outputs for fitting of measured Cd^{+2} contaminate breakthrough curves with adopted models at Ports 1, 2, and 3 for different inlet concentrations

Model	Parameter	C_o (mg/L)								
		Port 1			Port 2			Port 3		
		50	100	150	50	100	150	50	100	150
Bohart-Adams	KC_o	0.318	0.414	0.4528	0.319	0.441	0.487	0.284	0.371	0.376
	KN_oZ/U	2.424	2.585	2.323	3.782	3.771	3.374	3.694	3.826	3.008
	R^2	0.9848	0.988	0.9759	0.9925	0.9937	0.9907	0.9939	0.9929	0.9859
	SSE	0.1099	0.067	0.1110	0.0910	0.0630	0.0676	0.1729	0.0845	0.1174
Thomas-BDST	$KtCo$	0.318	0.414	0.4528	0.319	0.441	0.487	0.284	0.371	0.376
	$KtqM/Q$	2.424	2.585	2.323	3.782	3.771	3.374	3.694	3.826	3.008
	R^2	0.9848	0.988	0.9759	0.9925	0.9937	0.9907	0.9939	0.9929	0.9859
	SSE	0.1099	0.067	0.1110	0.0910	0.0630	0.0676	0.1729	0.0845	0.1174
Yan	$0.001QC/q_eM$	0.000	0.000	0.0003	0.000	0.0000	0.000	0.000	0.000	0.000
	a	1453	795	467	1806	4962	1648	20215	4906	3166
	R^2	0.9785	0.964	0.9717	0.9327	0.9414	0.9564	0.9122	0.9373	0.9702
	SSE	0.4890	0.500	0.3260	2.0151	1.5584	0.9899	2.696	1.9149	0.9070
Belter-Cussler-Hu	σ	0.589	0.560	0.590	0.444	0.465	0.488	0.447	0.456	0.521
	T_o	16.434	12.79	11.07	20.17	15.14	12.68	22.188	17.98	15.48
	R^2	0.9834	0.990	0.9824	0.9897	0.9806	0.9820	0.9889	0.9817	0.9790
	SSE	0.1227	0.056	0.0806	0.1283	0.1908	0.1338	0.2581	0.2141	0.1781
Clark	A	0.610	9.918	1.038	10.93	2.910	1.210	7.357	1.850	0.092
	r	0.2395	0.398	0.353	0.271	0.334	0.357	0.233	0.273	0.265
	n	1.146	1.876	1.2423	1.549	1.239	1.152	1.463	1.1645	1.0175
	R^2	0.9882	0.988	0.9778	0.9932	0.9961	0.9941	0.9941	0.9959	0.9929
	SSE	0.0862	0.067	0.1034	0.0807	0.0368	0.0415	0.1502	0.0472	0.0575

Table 2. Outputs for fitting of measured Cd^{+2} contaminate breakthrough curves with adopted models at Ports 1, 2, and 3 for different flow rates

| Model | Parameter | Flow Rate (mL/min) | | | | | |
| | | Port 1 | | Port 2 | | Port 3 | |
		10	15	10	15	10	15
Bohart-Adams	KC_o	0.474	0.560	0.448	0.5477	0.369	0.406
	KN_oZ/U	2.462	2.6307	3.2442	2.8366	3.471	2.778
	R^2	0.9845	0.9895	0.9920	0.9871	0.98984	0.98735
	SSE	0.0851	0.0499	0.06128	0.07408	0.09843	0.0966
Thomas-BDST	$KtCo$	0.474	0.560	0.448	0.5477	0.369	0.406
	$KtqM/Q$	2.462	2.6307	3.2442	2.8366	3.471	2.778
	R^2	0.9845	0.9895	0.9920	0.9871	0.98984	0.98735
	SSE	0.0851	0.0499	0.06128	0.07408	0.09843	0.0966
Yan	$0.001QC/q_eM$	0.000	0.0003	0.000	0.0002	0.000	0.0005
	a	380	468	1604	587	11211	171.6
	R^2	0.9871	0.9735	0.9595	0.97859	0.94898	0.9914
	SSE	0.3575	0.4063	0.97050	0.53711	1.40135	1.595
Belter-Cussler-Hu	σ	0.600	0.566	0.4998	0.553	0.4711	0.558
	T_o	11.514	9.785	13.49	10.610	16.722	14.09
	R^2	0.9750	0.9868	0.98554	0.97593	0.98557	0.9788
	SSE	0.1404	0.0646	0.11438	0.140071	0.14321	0.1650
Clark	A	0.0097	1.8759	3.2663	0.1062	1.3914	0.0424
	r	0.3474	0.447	0.3549	0.393	0.2718	0.2916
	n	1.002	1.3167	1.3434	1.021	1.1616	1.0092
	R^2	0.9930	0.99184	0.9939	0.99453	0.9930	0.9932
	SSE	0.0365	0.03943	0.0470	0.03063	0.06554	0.05038

6. CONCLUSION

1. The effective green production of (Ca/Al) nanoparticles was caused by the reaction of calcium derived from plaster kiln dust residue with aluminum resulted from alum dissolution in presence of CTAB surfactant. The capacity of coated slag to reclaim groundwater containing lead and cadmium ions has been proven by the precipitation of particles on the surfaces of iron-slag.
2. To produce a novel sorbent with high adsorptive capacities, (Ca/Al) molar ratio 2 at pH 10 is required, as well as CTAB mass 0.035 g/50 mL, slag dosage 1 g/50 mL, and LDH nanoparticles.
3. Characterization studies showed that slag coating was properly accomplished due to increases in Ca^{+2} and Al^{+3} percentages, as well as modification of slag, which can be linked with a substantial increase in surface area from 0.488 to 10.21 m^2/g. Additionally, a FESEM test showed that the produced sorbent was made of irregularly sized and oriented micrometric plates that were loosely combined.
4. The findings of continuous tests showed that the shape of breakthrough curves, as well as the values of breakthrough time, saturation time, and adsorbed quantities of metals within packed bed, are all significantly influenced by inlet metal concentration, velocity of flow, and quantity of coated slag. The emergence and spread of metal fronts along the length of the bed can be slowed down by decreasing input concentration and flow rate with rising bed depth, extending the life of the barrier.
5. The measured breakthrough curves were simulated with a high accuracy by models of Bohart-Adams, Thomas-BDST, Belter-Cussler-Hu, and Clark ($R^2>0.99$ and SSE<0.162). Results signified that the voids in the coated slag bed have not loss their ability to transport of contaminated water with average value of hydraulic conductivity coefficient of 2.7×10^{-2} cm/s.

REFERENCES

[1] Hou, D., O'Connor, D., Igalavithana, A.D., Alessi, D.S., Luo, J., Tsang, D.C.W., Sparks, D.L., Yamauchi, Y., Rinklebe, J., Ok, Y.S. (2020). Metal contamination and bioremediation of agricultural soils for food safety and sustainability. Nature Reviews Earth & Environment, 1: 366-381. https://doi:10.1038/s43017-020-0061-y

[2] Yousaf, B., Amina, Liu, G.J., Wang, R.W., Imtiaz, M., Rizwan, M.S., Zia-ur-Rehman, M., Qadir, A., Si, Y. (2016). The importance of evaluating metal exposure and predicting human health risks in urban–periurban environments influenced by emerging industry. Chemosphere, 150: 79-89. https://doi.org/10.1016/j.chemosphere.2016.02.007

[3] O'Connor, D., Hou, D., Ok, Y.S., Lanphear, B.P. (2020). The effects of iniquitous lead exposure on health. Nature Sustainability, 3: 77-79. https://doi:10.1038/s41893-020-0475-z

[4] Wang, L., Jin, Y., Weiss, D.J., Schleicher, N.J., Wilcke, W., Wu, L., Guo, Q., Chen, J., O'Connor, D., Hou, D. (2021). Possible application of stable isotope compositions for the identification of metal sources in soil. Journal of Hazardous Materials, 407: 124812. https://doi.org/10.1016/j.jhazmat.2020.124812

[5] Sahmoune, M.N., Louhab, K., Boukhiar, A. (2009). Biosorption of Cr (III) from aqueous solutions using bacterium biomass Streptomyces rimosus. International Journal of Environmental Research, 3(2): 229-238.

[6] Wang, S.L., Nan, Z.R., Li, Y., Zhao, Z.J. (2009). The

chemical bonding of copper ions on kaolin from Suzhou, China. Desalination, 249(3): 991-995. https://doi.org/10.1016/j.desal.2009.09.017

[7] Faisal, A.A.H., Al-Ridah, Z.A., Naji, L.A., Naushad, M., El-Serehy, H.A. (2020). Waste foundry sand as permeable and low permeable barrier for restriction of the propagation of lead and nickel ions in groundwater. Journal of Chemistry, 2020: 4569176. https://doi.org/10.1155/2020/4569176

[8] Goh, K.H., Lim, T.T., Dong, Z.L. (2008). Application of layered double hydroxides for removal of oxyanions: A review. Water Research, 42(6-7): 1343-1368. https://doi.org/10.1016/j.watres.2007.10.043

[9] Liang, X.F., Zang, Y.B., Xu, Y.M., Tan, X., Hou, W.G., Wang, L., Sun, Y.B. (2013). Sorption of metal cations on layered double hydroxides. Colloids and Surfaces A: Physicochemical and Engineering Aspects, 433: 122-131. https://doi.org/10.1016/j.colsurfa.2013.05.006

[10] Bo, A., Sarina, S., Liu, H.W., Zheng, Z.F., Xiao, Q., Gu, Y.T., Ayoko, G.A., Zhu, H.Y. (2016). Efficient removal of cationic and anionic radioactive pollutants from water using hydrotalcite-based getters. ACS Appl. Mater. Interfaces, 8: 16503-16510. https://doi.org/10.1021/acsami.6b04632

[11] Ahmed, D.N., Naji, L.A., Faisal, A.A.H., Al-Ansari, N., Naushad, M. (2020). Waste foundry sand/MgFe-layered double hydroxides composite material for efficient removal of Congo red dye from aqueous solution. Scientific Reports, 10: 2042. https://doi.org/10.1038/s41598-020-58866-y

[12] Colangelo, F., Cioffi, R. (2013). Use of cement kiln dust, blast furnace slag and marble sludge in the manufacture of sustainable artificial aggregates by means of cold bonding pelletization. Materials (Basel), 6(8): 3139-3159. https://doi.org/10.3390/ma6083139

[13] Green-Ruiz, C. (2009). Effect of salinity and temperature on the adsorption of Hg (II) from aqueous solutions by a Ca-montmorillonite. Environmental Technology, 30(1): 63-68. https://doi.org/10.1080/09593330802503859

[14] Yan, G., Viraraghavan, T., Chen, M. (2001). A new model for heavy metal removal in a biosorption column. Adsorption Science & Technology, 19(1): 25-43. https://doi.org/10.1260/0263617011493953

[15] John Thomas, W., Crittenden, B. (2004). Adsorption Technology and Design. Butterworth-Heinemann.

[16] Chu, K.H., Feng, X., Kim, E.Y., Hung, Y.T. (2011). Biosorption parameter estimation with genetic algorithm. Water, 3(1): 177-195. https://doi.org/10.3390/w3010177

[17] Chatterjee, A., Schiewer, S. (2011). Biosorption of cadmium (II) ions by citrus peels in a packed bed column: Effect of process parameters and comparison of different breakthrough curve models. CLEAN - Soil, Air, Water, 39(9): 874-881. https://doi.org/10.1002/clen.201000482

[18] Clark, R.M. (1987). Evaluating the cost and performance of field-scale granular activated carbon systems. Environmental Science & Technology, 21(6): 573-580. https://doi.org/10.1021/es00160a008

[19] Medvidović, N.V., Perić, J., Trgo, M. (2008). Testing of breakthrough curves for removal of lead ions from aqueous solutions by natural zeolite‐clinoptilolite according to the Clark kinetic equation. Separation Science and Technology, 43(4): 944-959. https://doi.org/10.1080/01496390701870622

[20] Mierczynska-Vasilev, A., Smith, P.A. (2016). Surface modification influencing adsorption of red wine constituents: The role of functional groups. Applied Surface Science, 386: 14-23. https://doi.org/10.1016/j.apsusc.2016.06.016

[21] Saha, S., Ray, S., Ghosh, S., Chakraborty, J. (2018). pH-dependent facile synthesis of CaAl-layered double hydroxides and its effect on the growth inhibition of cancer cells. Journal of the American Ceramic Society, 101(9): 3924-3935. https://doi.org/10.1111/jace.15555

[22] Xu, Z.P., Zeng, H.C. (2001). Abrupt structural transformation in hydrotalcite-like compounds $Mg_{1-x}Al_x(OH)_2(NO_3)_x \cdot n\ H_2O$ as a continuous function of nitrate anions. The Journal of Physical Chemistry B, 105(9): 1743-1749. https://doi.org/10.1021/jp0029257

[23] Guo, Y.W., Zhu, Z.L., Qiu, Y.L., Zhao, J.F. (2012). Adsorption of arsenate on Cu/Mg/Fe/La layered double hydroxide from aqueous solutions. Journal of Hazardous Materials, 239-240: 279-288. https://doi.org/10.1016/j.jhazmat.2012.08.075

[24] Ahmed, D.N., Faisal, A.A.H., Jassam, S.H., Naji, L.A., Naushad, M. (2020). Kinetic model for pH variation resulted from interaction of aqueous solution contaminated with nickel ions and cement kiln dust. Journal of Chemistry, 2020: 8732308. https://doi.org/10.1155/2020/8732308

[25] Liu, L.P., Cui, X.M., Qiu, S.H., Yu, J.L., Zhang, L. (2010). Preparation of phosphoric acid-based porous geopolymers. Applied Clay Science, 50(4): 600-603. https://doi.org/10.1016/j.clay.2010.10.004

[26] Amaniampong, P.N., Trinh, Q.T., Wang, B., Borgna, A., Yang, Y., Mushrif, S.H. (2015). Biomass oxidation: Formyl C-H bond activation by the surface lattice oxygen of regenerative CuO Nanoleaves. Angewandte Chemie International Edition, 54: 8928-8933. https://doi.org/10.1002/anie.201503916

[27] Amaniampong, P.N., Trinh, Q.T., Varghese, J.J., Behling, R., Valange, S., Mushrif, S.H., Jérôme, F. (2018). Unraveling the mechanism of the oxidation of glycerol to dicarboxylic acids over a sonochemically synthesized copper oxide catalyst. Green Chemistry, 12. https://https://doi.org/10.1039/c8gc00961a

[28] Chen, Q.Q., Yin, D.Q., Zhu, S.J., Hu, X.L. (2012). Adsorption of cadmium (II) on humic acid coated titanium dioxide. Journal of Colloid and Interface Science, 367(1): 241-248. https://doi.org/10.1016/j.jcis.2011.10.005

[29] Ko, D.C.K., Porter, J.F., McKay, G. (2000). Optimised correlations for the fixed-bed adsorption of metal ions on bone char. Chemical Engineering Science, 55(23): 5819-5829. https://doi.org/10.1016/S0009-2509(00)00416-4

[30] Kundu, S., Gupta, A.K. (2007). As (III) removal from aqueous medium in fixed bed using iron oxide-coated cement (IOCC): Experimental and modeling studies. Chemical Engineering Journal, 129(1-3): 123-131. https://doi.org/10.1016/j.cej.2006.10.014

[31] Liao, P., Zhan, Z.Y., Dai, J., Wu, X.H., Zhang, W.B., Wang, K., Yuan, S.H. (2013). Adsorption of tetracycline and chloramphenicol in aqueous solutions by bamboo charcoal: A batch and fixed-bed column study. Chemical Engineering Journal, 228: 496-505. https://doi.org/10.1016/j.cej.2013.04.118

[32] Marzbali, M.H., Esmaieli, M. (2017). Fixed bed adsorption of tetracycline on a mesoporous activated carbon: Experimental study and neuro-fuzzy modeling.

NOMENCLATURE

C	Solute concentration, mg/l
C/Co	Normalized concentration
Ce	The equilibrium concentration, mg/l
C_o	Initial concentration of pollutant, mg/l
R^2	Coefficient of determination

Greek symbols

α_L	Longitudinal dispersivity, cm
ρ_b	Bulk density of the soil, g/cm^3
τ	Tortuosity factor of soil medium
ω	Tortuosity

Subscripts

ADE	Advection-dispersion equation
BET	Batch Equilibrium Technique
FESEM	Scanning Electron Microscopy
ITRC	Interstate Technology & Regulatory Council
XRD	X-Ray Diffraction
EDS	Energy-dispersive X-ray spectroscopy
FTIR	Fourier-transform infrared spectroscopy
NPs	nanoparticles
P	Port
PDE	Partial Differential Equation
SSE	Sum squared errors
PRBs	Permeable Reactive Barriers
LDHs	Layered Double Hydroxides
MMT	Montmorillonite
CTAB	Cetyl Trimethyl Ammonium Bromide
PKD	Plaster Kiln Dust